Modulation of the two-dimensional electron gas channel in flexible AlGaN/GaN highelectron-mobility transistors by mechanical bending

Cite as: Appl. Phys. Lett. 116, 123501 (2020); https://doi.org/10.1063/1.5142546 Submitted: 18 December 2019 . Accepted: 06 March 2020 . Published Online: 23 March 2020

Weijie Wang, Jie Chen, James Spencer Lundh 🗓, Shahab Shervin 🗓, Seung Kyu Oh, Sara Pouladi, Zhoulyu Rao, Ja Yeon Kim, Min-Ki Kwon, Xiaohang Li 🗓, Sukwon Choi 🗓, and Jae-Hyun Ryou 🗓

COLLECTIONS

EP This paper was selected as an Editor's Pick













Cite as: Appl. Phys. Lett. **116**, 123501 (2020); doi: 10.1063/1.5142546 Submitted: 18 December 2019 · Accepted: 6 March 2020 · Published Online: 23 March 2020







Weijie Wang,^{1,2} Jie Chen,^{1,2,3} James Spencer Lundh,⁴ D Shahab Shervin,^{1,2} D Seung Kyu Oh,^{1,2} Sara Pouladi,^{2,3} Zhoulyu Rao,¹ Ja Yeon Kim,⁵ Min-Ki Kwon,⁶ Xiaohang Li,⁷ D Sukwon Choi,⁴ D and Jae-Hyun Ryou^{1,2,3,a)} D

AFFILIATIONS

- Department of Mechanical Engineering, University of Houston, Houston, Texas 77204-4006, USA
- ²Texas Center for Superconductivity at UH (TcSUH) and Advanced Manufacturing Institute (AMI), University of Houston, Houston, Texas 77204, USA
- ³Materials Science and Engineering Program, University of Houston, Houston, Texas 77204, USA
- Department of Mechanical Engineering, The Pennsylvania State University, University Park, Pennsylvania 16802, USA
- ⁵Korea Photonics Technology Institute (KOPTI), Gwangju 61007, South Korea
- ⁶Department of Photonic Engineering, Chosun University, Gwangju 61452, South Korea
- ⁷Advanced Semiconductor Laboratory, King Abdullah University of Science and Technology (KAUST), Thuwal 23955, Saudi Arabia

ABSTRACT

We investigate the effect of strain on the two-dimensional electron gas (2DEG) channel in a flexible $Al_{0.25}Ga_{0.75}N/GaN$ high-electron-mobility transistor (HEMT) by mechanical bending to prove the concept of active polarization engineering to create multifunctional electronic and photonic devices made of flexible group III-nitride thin films. The flexible HEMTs are fabricated by a layer-transfer process and integrated with a 150- μ m-thick Cu film. The strain values are estimated from high-resolution x-ray diffraction and Raman spectroscopy in 4-cm bend-down and -4-cm bend-up test conditions. The strain-induced piezoelectric polarization can alter the charge density of the 2DEG in the channel at the AlGaN/GaN interface and thus modify the output characteristics of the flexible HEMTs. Accordingly, output characteristics show an increase in output current by 3.4% in the bend-down condition and a decrease by 4.3% in the bend-up condition. Transfer characteristics show a shift of threshold voltage, which also supports the 2DEG channel modulation during bending. Computational simulation based on the same structure confirms the same current modulation effect and threshold voltage shift. Furthermore, the electrical characteristics of the flexible HEMTs show a repeatable dependence on the strain effect, which offers potential for electro-mechanical device applications.

Published under license by AIP Publishing. https://doi.org/10.1063/1.5142546

Mechanically flexible electronic and photonic devices based on group-III-nitride (III-N) thin films have been developed for potential system applications of wireless communication, radars, flexible displays, electro-mechanical sensing, and energy harvesting. ¹⁻⁴ Most of these studies focused on the mechanical bendability of the structure while minimizing the performance degradation of the devices, which is important in many applications. However, flexible devices made of III-N thin films have implications surpassing merely the ability to fabricate bendable devices. Owing to the unique piezoelectric properties of III-N materials, external strain applied during bending can be exploited to control device characteristics and to provide additional functionality. Shervin *et al.* have proposed strain-effect transistors,

suggesting that the transfer characteristics and operation mode of III-N high-electron-mobility transistors (HEMTs) can be modified by external bending without applying gate biases. Shervin *et al.* also suggested that controlled external bending can lead to improvements in internal quantum efficiency and emission wavelength tunability of light-emitting diodes (LEDs). Furthermore, as opposed to an n-type two-dimensional electron gas (2DEG) channel in HEMTs, Wang *et al.* demonstrated that the formation of a p-type two-dimensional hole gas (2DHG) channel is possible in flexible $In_xAl_{1-x}N/GaN$ heterostructures by bending, possibly enabling high-hole-mobility transistors. However, the aforementioned reports are only based on numerical modeling. No systematic study has been performed, which also

a) Author to whom correspondence should be addressed: jryou@uh.edu

experimentally demonstrates and proves the feasibility of such multifunctional electronic and photonic devices. For experimental demonstration, substantial controlled strain has to be applied in the device active region, which is challenging in the structures of typical flexible devices due to the low elastic modulus of commonly used flexible polymer substrates. In this case, the neutral plane of the structure during bending is within the III-N semiconductor layer (refer to the section entitled "Neutral plane of multi-layered structure" in the supplementary material), and thus, a significantly high degree of bending is necessary to achieve sufficient strain. However, these bending conditions cause mobility reduction and device degradation. Additionally, flexible HEMTs on a polymeric substrate suffer from significantly reduced current due to the self-heating effect, which limits their high-power applications in flexible electronics. 10,111 To overcome the challenges associated with experimentally proving the concept of multifunctional flexible III-N devices, a flexible substrate that possesses a high elastic modulus and high thermal conductivity is required. Flexible copper (Cu) substrates can satisfy this requirement as they offer both high elastic modulus (\sim 130 GPa) and high thermal conductivity (\sim 400 W/m K). It was previously demonstrated that the use of a Cu substrate for flexible HEMTs suppresses the self-heating effect. 12

The multifunctionality of flexible III-N electronic and photonic devices originates from the electronic band structure modification as a result of changes in piezoelectric charges at the heterostructure interface. Therefore, for the proof of concept, it is necessary to confirm that the electronic band structure and its associated device characteristics are changed according to the controlled strain imposed by external bending. The authors previously demonstrated that the electronic band structure in AlGaN/GaN HEMTs can be modified by the polarization modulation effect of a single-crystalline piezoelectric BeO cap layer, resulting in a 14% increase in the 2DEG density. 13 This previous report shows the feasibility of polarization engineering in III-N heterostructures, but not specifically for flexible devices. In the present study, we systematically investigate the changes in device characteristics from the band structure modification in flexible AlGaN/GaN HEMTs, which originates from the strain induced by bending in order to prove the concept of the proposed multifunctional devices enabled by active polarization engineering. The III-N heterostructure was epitaxially grown on a Si substrate to simplify the substrate removal process; this process has been demonstrated previously for the fabrication of flexible III-N thin film piezoelectric energy harvesters and sensors. 14,15 A similar process was applied to fabricate the flexible HEMTs on a Cu film in this study. We integrate the flexible HEMT with Cu by electroplating and achieve both high stiffness and high heat dissipation. Moreover, active current modulation by external strain is observed, which proves the concept of active polarization engineering in flexible III-N thin film heterostructures, which was not demonstrated in the previous studies.

The III-N HEMTs have a typical layer structure consisting of an $Al_{0.25}Ga_{0.75}N$ Schottky barrier layer (20 nm) and a GaN layer (2 μ m) on a Si (111) substrate with AlN and AlGaN buffer layers. A patterned stack of Ti/Al/Ni/Au (20/80/50/50 nm) metal layers was deposited by electron-beam evaporation followed by rapid thermal annealing at 850 °C in a nitrogen (N_2) atmosphere to form source and drain electrodes. Another patterned stack of Ni/Au (50/50 nm) metal layers was deposited between the source and drain to serve as a gate electrode. The HEMT-on-Si sample was first flipped over and attached to a

temporary sapphire carrier wafer. The Si substrate was then removed by wet etching. Cr/Au (10/200 nm) metal layers were deposited on the back surface of the III-N epitaxial structure that was exposed after substrate removal. Finally, a 150- μ m-thick Cu film was deposited on the Cr/Au layer by electroplating using $\rm CuSO_4$ electrolyte solution. All the deposited metal layers are expected to achieve a non-slip and void-free condition at the interfaces, unlike typical bonded interfaces. Therefore, a semiconductor heterostructure and a Cu plate were bent together as one body.

Figure 1 shows a schematic cross section of the flexible HEMT structure. A neutral plane, $y_{neutral}$ (indicated by a blue dotted line), is located around the middle of the Cu layer (refer to the section entitled "Neutral plane of multi-layered structure" in the supplementary material). In this case, the AlGaN/GaN heterostructure always experiences uniaxial in-plane external strain during bending. When the flexible structure on the Cu film is bent concavely with the radius of curvature R < 0 (defined as the bend-up condition in this study), in-plane compressive strain is applied in the III-N layer, i.e., $\varepsilon_{xx} < 0$. Conversely, when the flexible structure is bent convexly with R > 0 (bend-down condition), in-plane tensile strain is applied ($\varepsilon_{xx} > 0$). The bending radius was set at ± 4 cm. In such conditions, we believe that substantial strain can be induced in the 2DEG channel, while plastic deformation or device degradation is avoided. The reproducibility of bending was confirmed, and no current drop or change was observed after repeated bending cycles. The bending condition and its associated device characteristics were reproducible.

The strain applied in the GaN channel during bending was estimated from the lattice parameters measured by high-resolution x-ray diffraction (HR-XRD, Bruker, D8 Discover). Figure 2 shows the symmetric 2theta-omega scans in flat (black), bend-down (red), bend-up (blue), and re-flat (green) conditions. The bending direction is perpendicular to the x-ray diffraction plane to minimize the peak broadening caused by curved surfaces. For the bend-down condition ($R=4\,\mathrm{cm}$), the GaN (002) peak (\sim 34.6°) shifts to the right by 0.079° due to the reduction of the out-of-plane lattice constant c under in-plane tensile strain. Conversely, the GaN (002) peak shifts to the left by 0.087° in the bend-up condition ($R=-4\,\mathrm{cm}$). Asymmetric (102) plane 2theta-omega scans were also measured, and the lattice spacings $d_{(002)}$ and $d_{(102)}$ were calculated by the Bragg law. As shown in the inset of Fig. 2 (top right), rotational scans (phi scan) around (102) planes were measured and six peaks with 60° internal spacings in the flat condition

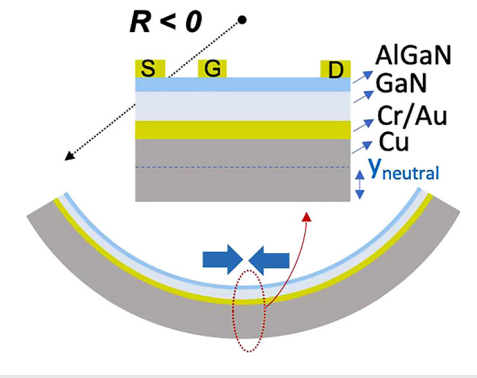


FIG. 1. Schematic cross-sectional structure of the flexible high-electron-mobility transistor (HEMT) and the bend-up test condition.

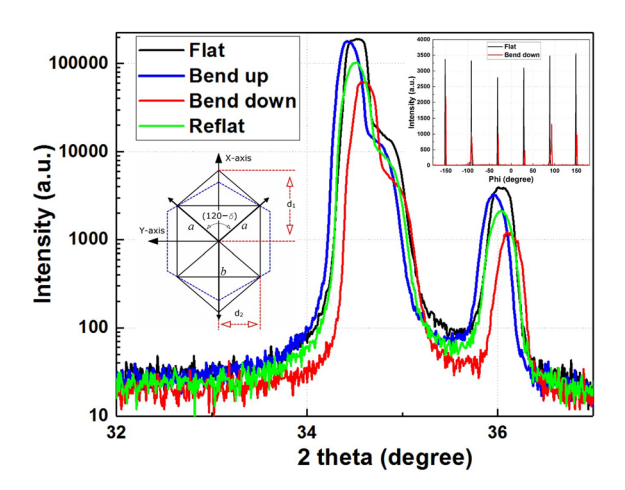


FIG. 2. Symmetric x-ray 2theta-omega scans of a flexible HEMT structure in flat (black), bend-down (red), bend-up (blue), and re-flat (green) test conditions. The insets show the orthorhombic distortion of the hexagonal biaxial plane under uniaxial strain (left) and rotational phi scans on the GaN {102} plane (top right).

(black) indicate the sixfold symmetry of the hexagonal GaN crystal structure. As shown in the left inset of Fig. 2, we assume that the uni-axial tensile stress in the x direction by 1-dimensional bending causes the orthorhombic distortion of the hexagonal biaxial plane ($a \neq b$) with a distortion angle of $\delta \approx 0.36^{\circ}$. The lattice constants a and b of the distorted biaxial plane can be calculated by

$$\frac{1}{d_{(102)}^2} = \frac{1}{a^2 \sin^2(120 - \delta)} + \frac{4}{c^2},\tag{1}$$

$$b = \frac{2a\sin(120 - \delta)}{\sqrt{2(1 - \cos(120 - \delta))}},$$
 (2)

where a is calculated to be 0.3178 nm and b to be 0.3196 nm. Thus, the anisotropic strain values can be calculated by 17

$$\begin{cases} \varepsilon_{xx} = (d_1 - d_{10})/d_{10}, \\ \varepsilon_{yy} = (d_2 - d_{20})/d_{20}, \\ \varepsilon_{zz} = (c - c_0)/c_0, \end{cases}$$
(3)

where $d_1 = b$, $d_{10} = a_0$, $d_2 = a\sin(120 - \delta)/\sqrt{2(1 + \cos(120 - \delta))}$, and $d_{20} = \sqrt{3}a_0/2$. a_0 and c_0 are the lattice constants of GaN without distortion at the flat condition. Table I summarizes the calculated lattice constants and strains in different bending conditions. For the 4-cm bend-down condition, in-plane strain values of $\varepsilon_{xx} = 0.57\%$ and $\varepsilon_{yy} = -0.18\%$ are calculated. Similarly, for the 4-cm bend-up condition, in-plane strain values of $\varepsilon_{xx} = -0.59\%$ and $\varepsilon_{yy} = 0.21\%$ are calculated. Raman spectroscopy was also performed with a Horiba LabRAM HR Evolution spectrometer using 532nm excitation in a 180° backscattering configuration. The in-plane strain values of 0.09% in the bend-down condition and -0.13% in the bend-up condition are calculated (refer to the section entitled "Uniaxial strain measurement by Raman spectroscopy" in the supplementary material).

I-V characteristics of the flexible HEMTs in various bending conditions were then measured. The device dimensions include a gate length of $L_g=10~\mu\mathrm{m}$, a gate–drain distance of $L_{gd}=30~\mu\mathrm{m}$, a gate-source distance of $L_{gs}=15~\mu\mathrm{m}$, and a channel width of $W_g=100~\mu\mathrm{m}$.

TABLE I. HR-XRD results and calculated strain based on the orthorhombic distortion of the hexagonal biaxial plane under uniaxial strain at flat, bend-down, bend-up, and re-flat conditions.

	d ₁₀₂ (Å)	c (Å)	a (Å)	b (Å)	ε_{xx}	ε_{yy}	ϵ_{zz}
Flat	1.889	5.1968	3.1783	3.1783			
Bend-down	1.890	5.1853	3.1781	3.1964	0.57%	-0.18%	0.22%
Bend-up	1.888	5.2110	3.1786	3.1597	-0.59%	0.21%	-0.25%
Re-flat	1.889	5.1983	3.1770	3.1770	-0.04%	-0.04%	0.03%

Figure 3 shows the I_{ds} - V_{ds} characteristics of a flexible HEMT in the flat (black), bend-down (red), bend-up (blue), and re-flat (green) conditions with no applied gate voltage ($V_g = 0 \, \text{V}$). The bending direction is perpendicular to the source-to-drain direction to avoid decreased mobility resulting from the channel curvature, 19,20 as shown in the insets of Fig. 3. Data from the first (solid circle) and second (hollow circle) bending cycle show a good repeatability of the strain effect in the flexible HEMT. Current modulation by the applied strain is observed. The saturation current I_{ds} at $V_{ds}=20\,\mathrm{V}$ is measured to be 74.6 mA, 77.1 mA, 75.1 mA, 71.0 mA, 77.2 mA, 75.3 mA, and 72.2 mA in the flat, first bend-down, first re-flat, first bend-up, second benddown, second re-flat, and second bend-up conditions, respectively. The average changes in the saturation current are 3.4% for the benddown condition and -4.3% for the bend-up condition. Moreover, the changes in threshold voltage in transfer characteristics are observed (refer to the section entitled "Transfer characteristics of flexible HEMT by bending" in the supplementary material).

Computational simulation based on this structure was performed.²¹ Minor discrepancies were observed between the strain values measured by HR-XRD and Raman spectroscopy. Since HR-XRD is more sensitive to the strain near the surface close to the 2DEG,

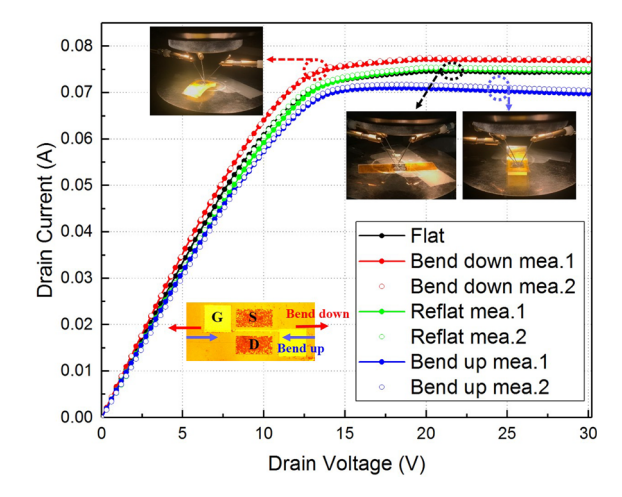


FIG. 3. Output characteristics (I_{ds} – V_{ds}) of a flexible HEMT in flat (black), benddown (red), re-flat (green), and bend-up (blue) test conditions during the first (solid circle) and second (hollow circle) bending cycles. The top insets show the measurement setup for each bending condition. The bottom inset shows an optical photomicrograph of the HEMT device and the direction of in-plane strain in the bend-up and bend-down test conditions.

strain values of $\varepsilon_{xx} + \varepsilon_{yy} = 0.39\%$ and $\varepsilon_{xx} + \varepsilon_{yy} = -0.38\%$ from HR-XRD were used for the modeling of the flexible AlGaN/GaN HEMT. Figure 4 shows simulated output characteristics of the flexible HEMT with different bending conditions. The 2DEG mobility is set to $1200 \, \mathrm{cm}^2/\mathrm{V}$ s, and the change in mobility due to the altered effective mass during bending is considered to be negligible. The change in I_{ds} shows a typical depletion-mode n-type channel and decreases with more negative gate bias. Source–drain current I_{ds} can be modified by the applied strain at different gate voltages. For $V_g = 0 \, \mathrm{V}$, saturation I_{ds} increases by 4.33% for the 4-cm bend-down condition and decreases by 4.29% for the -4-cm bend-up condition. The strain-induced change in current from simulation agrees well with the experimental results in both the transfer and output characteristics, which confirms the current modulation effect from the applied strain.

The origin of this current modulation effect is due to the change in the 2DEG density when strain is applied. The general expression for sheet charge density in a HEMT device is given by²³

$$n_s = \sigma_{pol} - \frac{\varepsilon_{AlGaN}}{q \cdot d_{AlGaN}} [\phi_{Bn} + E_F(n_s) - \Delta E_C], \tag{4}$$

where σ_{pol} is the total spontaneous and piezoelectric polarization induced charge concentration, ε_{AlGaN} and d_{AlGaN} are the permittivity and thickness of the AlGaN barrier layer, q is the electron charge, ϕ_{Bn} is the Schottky barrier, and $E_F(n_s)$ and ΔE_C are the quantum well depth and conduction band offset at the AlGaN/GaN interface, respectively. ϕ_{Bn} is a strong function of both strain and interface state density. However, the leakage current $(I_{gs}-V_{gs})$ was measured at different bending conditions and there was no observable change with positive gate bias, which indicates that the Schottky barrier height is not changed. This could be related to an increased surface state density as a result of strain induced defects when bending is applied, which offsets the strain effect on the Schottky barrier height.²² The change in the 2DEG density Δn_s is then simplified as a change in polarization charge $\Delta\sigma_{pol}$ during bending. $\Delta\sigma_{pol}$ can be calculated as $-\Delta\sigma_{pol}$ $=\nabla\cdot(\Delta P_{pz})^{25}$, where ΔP_{pz} , which is the additional piezoelectric polarization field during 1D bending, can be calculated as

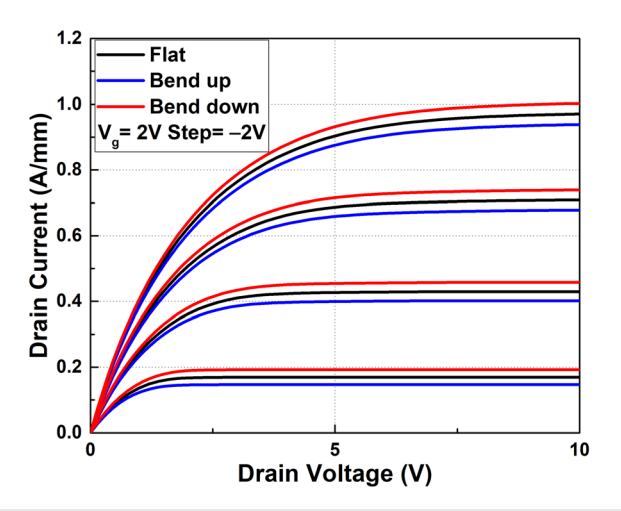


FIG. 4. Simulated output characteristics (I_{ds} – V_{ds}) of a flexible HEMT in flat (black), bend-down (red), and bend-up (blue) test conditions.

$$\Delta P_{pz} = \left[e_{31}(\varepsilon_{xx} + \varepsilon_{yy}) + e_{33}\varepsilon_{zz} \right]_{AlGaN}$$

$$- \left[e_{31}(\varepsilon_{xx} + \varepsilon_{yy}) + e_{33}\varepsilon_{zz} \right]_{GaN},$$
 (5)

where e_{31} , e_{33} are the piezoelectric constants of GaN and Al_{0.25}Ga_{0.75}N.^{26,27} Adopting the uniaxial tensile strain in the 4-cm bend-down condition ($\varepsilon_{yy}=0.57\%$, $\varepsilon_{yy}=-0.18\%$, $\varepsilon_{zz}=-0.22\%$), ΔP_{pz} is found to be -5.09×10^{-4} C/m². This additional negative piezoelectric polarization field can induce more positive polarization charge $\Delta \sigma_{pol}$ at the interface and attract a higher level of sheet electron density. A greater negative gate voltage is needed to fully deplete this enhanced 2DEG channel, and thus, a negative shift of threshold voltage is observed (refer to the section entitled "Transfer characteristics of flexible HEMT by bending" in the supplementary material). Conversely, when uniaxial compressive strain is applied in the -4-cm bend-up condition ($\varepsilon_{yy}=-0.59\%$, $\varepsilon_{yy}=0.21\%$, $\varepsilon_{zz}=0.25\%$), ΔP_{pz} is found to be 5.61×10^{-4} C/m². Additional negative polarization charge is formed and thus reduces the 2DEG sheet concentration and shifts the threshold voltage in the positive direction.

In summary, we studied the strain effect in a flexible Al_{0.25}Ga_{0.75}N/GaN HEMT via both numerical simulation and experimental demonstration. The flexible HEMTs were fabricated by a layer-transfer process and integrated with a 150-μm-thick Cu film by electroplating. HR-XRD was used to estimate in-plane strains of ε_{xx} = 0.57%, ε_{yy} = -0.18% and ε_{xx} = 0.59%, ε_{yy} = -0.21% for 4-cm bend-down and -4-cm bend-up test conditions, respectively. From the measured output characteristics, current changes of 3.4% and -4.3% were observed in the bend-down and bend-up test conditions, respectively. Threshold voltage shifts were also observed, which indicated changes in the 2DEG sheet density in the channel during bending. Computational simulation was performed, where a 4.3% current modulation was demonstrated. The origin of current modulation was discussed, and we believe that piezoelectric polarization charge induced by the applied strain altered the 2DEG density in the channel and thus resulted in changes in the drain current. Even greater changes in the polarization charge and more current modulation can be expected if InAlN with larger negative piezoelectric constants is used as the barrier layer. This strain effect of the flexible HEMTs offers the potential for wearable electro-mechanical devices for sensor, transducer, and actuator applications.

See the supplementary material for the complete neutral plane calculation, strain measurements by Raman spectroscopy, and transfer characteristics with bending.

This material is based upon the work at the University of Houston supported by the National Science Foundation under Grant No. 1842299 [Electrical, Communications and Cyber Systems (ECCS)] and the King Abdullah University of Science and Technology (KAUST), Saudi Arabia (Contract No. OSR-2017-CRG6-3437.02). J.H.R. also acknowledges partial support from the Texas Center for Superconductivity at the University of Houston (TcSUH) and Advanced Manufacturing Institute (AMI). Funding for efforts by the Pennsylvania State University was provided by the AFOSR Young Investigator Program (Grant No. 265 FA9550-17-1-0141, Program Officers: Dr. Brett Pokines, and Dr. Michael Kendra, also monitored by Dr. Kenneth Goretta).

REFERENCES

- ¹C.-W. Sher, K.-J. Chen, C.-C. Lin, H.-V. Han, H.-Y. Lin, Z.-Y. Tu, H.-H. Tu, K. Honjo, H.-Y. Jiang, S.-L. Ou, R.-H. Horng, X. Li, C.-C. Fu, and H.-C. Kuo, Opt. Express 23. A1167 (2015).
- ²A. Vinel, W. S. E. Chen, N. N. Xiong, S. Rho, N. Clilamkurti, and A. V. Vasilaks, IEEE Wireless Commun. 23, 8 (2016).
- ³N. Petrone, I. Meric, T. Chari, K. L. Shepard, and J. Hone, IEEE J. Electron Devices Soc. 3, 44 (2015).
- ⁴Y. H. Jung, H. Zhang, S. J. Cho, and Z. Ma, IEEE Trans. Electron Devices **64**, 1881 (2017).
- ⁵S. Shervin, S.-H. Kim, M. Asadirad, S. Ravipati, K.-H. Lee, K. Bulashevich, and J.-H. Ryou, Appl. Phys. Lett. **107**, 193504 (2015).
- ⁶S. Shervin, S. K. Oh, H. J. Park, K.-H. Lee, M. Asadirad, S. H. Kim, J. Kim, S. Pouladi, S.-N. Lee, X. Li, J. S. Kwak, and J.-H. Ryou, J. Phys. D **51**, 105105 (2018).
- 7S. Shervin, S.-H. Kim, M. Asadirad, S. Y. Kapov, D. Zimina, and J.-H. Ryou, ACS Photonics 3, 486 (2016).
- ⁸W. Wang, S. Shervin, S. K. Oh, J. Chen, Y. Huai, S. Pouladi, H. Kim, S.-N. Lee, and J.-H. Ryou, IEEE Electron Device Lett. **38**, 1086 (2017).
- ⁹N. R. Glavin, K. D. Chabak, E. R. Heller, E. A. Moore, T. A. Prusnick, B. Maruyama, D. E. Walker, Jr., D. L. Dorsey, Q. Paduano, and M. Snure, Adv. Mater. 29, 1701838 (2017).
- ¹⁰ K. J. Lee, M. A. Meitl, J. H. Ahn, J. A. Rogers, R. G. Nuzzo, V. Kumar, and I. Adesida, J. Appl. Phys. **100**, 124507 (2006).
- ¹¹M. Lesecq, V. Hoel, A. Lecavelier des Etangs-Levallois, E. Pichonat, Y. Douvey, and J. C. De Jaeger, IEEE Electron Device Lett. 32, 143 (2011).
- ¹²S. K. Oh, M. U. Cho, J. Dallas, T. Jang, D. G. Lee, S. Pouladi, J. Chen, W. Wang, S. Shervin, H. Kim, S. Shin, S. Choi, J. S. Kwak, and J.-H. Ryou, Appl. Phys. Lett. 111, 133502 (2017).

- ¹³W. Wang, S. M. Lee, S. Pouladi, J. Chen, S. Shervin, S. Yoon, J. H. Yum, E. S. Larsen, C. W. Bielawski, B. Chatterjee, S. Choi, J. Oh, and J.-H. Ryou, Appl. Phys. Lett. 115, 103502 (2019).
- ¹⁴J. Chen, S. K. Oh, N. Nabulsi, H. Johnson, W. Wang, and J.-H. Ryou, Nano Energy 57, 670 (2019).
- ¹⁵J. Chen, H. Liu, W. Wang, N. Nabulsi, W. Zhao, J. Y. Kim, M.-K. Kwon, and J.-H. Ryou, Adv. Funct. Mater. 29, 1903162 (2019).
- ¹⁶A. P. Boresi and R. J. Schmidt, Advanced Mechanics of Materials, 6th ed. (Wiley, Hoboken, NJ, USA, 2002).
- ¹⁷M. R. Laskar, T. Ganguli, A. A. Rahman, A. Mukherjee, N. Hatui, M. R. Gokhale, and A. Bhattacharya, J. Appl. Phys. 109, 013107 (2011).
- A. Bansal, K. Wang, J. S. Lundh, S. Choi, and J. M. Redwing, Appl. Phys. Lett. 114, 142101 (2019).
- ¹⁹Y. Gao, M. Asadirad, Y. Yao, P. Dutta, E. Galstyan, S. Shervin, K.-H. Lee, S. Pouladi, S. Sun, Y. Li, M. Rathi, J.-H. Ryou, and V. Selvamanickam, ACS Appl. Mater. Interfaces 8, 29565 (2016).
- ²⁰M. Asadirad, S. Pouladi, S. Shervin, S. K. Oh, K. H. Lee, J. Kim, S.-N. Lee, Y. Gao, P. Dutta, V. Selvamanickam, and J.-H. Ryou, IEEE Electron Device Lett. 38, 217 (2017).
- ²¹See http://www.str-soft.com/products/FETIS for "Capabilities and Brief Physical Model."
- ²²C. E. Dreyer, A. Janotti, and C. G. Van de Walle, Appl. Phys. Lett. **102**, 142105 (2013).
- ²³K. Yao, S. Khandelwal, F. Sammoura, A. Kazama, C. Hu, and L. Lin, IEEE Electron Device Lett. 36, 902 (2015).
- ²⁴A. Wang, L. Zeng, and W. Wang, Mater. Res. Express 5, 025903 (2018).
- 25 E. T. Yu, X. Z. Dang, P. M. Asbeck, S. S. Lau, and G. J. Sullivan, J. Vac. Sci. Technol., B 17, 1742 (1999).
- ²⁶J.-H. Ryou, P. D. Yoder, J. Liu, Z. Lochner, H. Kim, S. Choi, H. J. Kim, and R. D. Dupuis, IEEE J. Sel. Top. Quantum Electron. 15, 1080 (2009).
- ²⁷J. Kuzmik, Semicond. Sci. Technol. 17, 540 (2002).